processes

MDPI

Article

Aluminium-Assisted Alloying of Carbon Steel in Submerged Arc Welding: Application of Al-Cr-Ti-Cu Unconstrained Metal Powders

Theresa Coetsee * and Frederik De Bruin

Department of Materials Science and Metallurgical Engineering, University of Pretoria, Pretoria 0002, South Africa; fjdb.1953@gmail.com
* Correspondence: theresa.coetsee@up.ac.za

Abstract: Al assisted alloying of carbon steel in Submerged Arc Welding (SAW) by Al-Cr-Ti-Cu unconstrained metal powders is applied. A base case without metal powder additions is compared to two metal powder addition schedules, Al-Cu-Ti and Al-Cu-Ti-Cr. Al powder is used as a deoxidiser element to control the oxygen partial pressure at the weld pool–molten flux interface to ensure that most of the Ti and Cr metal powder is transferred into the weld pool and that the weld metal ppm O is controlled within acceptable limits of 200 to 500 ppm O. The likely sequence of alloy melt formation is deduced from the relevant alloy phase diagrams. The effect of Fe addition into the initial Al-Cu-Ti and Al-Cu-Ti-Cr alloy melt is illustrated in thermochemical calculations. Increased metal deposition productivity with metal powder addition in SAW is confirmed. The metal deposition rates increased by 19% and 40% when Al-Cu-Ti and Al-Cu-Ti-Cr powders were applied at the same weld heat input used in the absence of metal powder additions.

Keywords: oxygen potential; titanium; aluminium; copper; chromium; metal powder; submerged arc welding

Citation: Coetsee, T.; De Bruin, F. Aluminium-Assisted Alloying of Carbon Steel in Submerged Arc Welding: Application of Al-Cr-Ti-Cu Unconstrained Metal Powders. *Processes* **2022**, *10*, 452. https://doi.org/10.3390/pr10030452

Academic Editor: Prashant K Sarswat

Received: 26 January 2022
Accepted: 22 February 2022
Published: 24 February 2022

1. Introduction

Submerged Arc Welding (SAW) is a high productivity welding method used in heavy engineering industries to join thick steel plates together to build large structures, for example, container ships [1]. Heat input in the SAW process is made via an arc formed between the weld wire tip and the steel base plate. The arc is covered by a layer of molten flux (slag) formed from melting the unmelted flux cover positioned at the edge of the arc cavity. The weld wire and flux are continuously fed through the welding head arrangement. The welding head is attached to a moving carriage which travels along the weld length. As the weld wire is fed into the arc cavity, the weld wire is melted into metal droplets which transfer via the arc plasma–weld pool interface into the weld pool. Complex physical and chemical interactions of heat and mass transfer occur in the arc cavity [1,2]. Chemical reactions continue in the trailing molten steel weld pool and its covering molten flux layer until the steel is solidified as weld metal [3,4]. SAW fluxes include both fluorides and oxides. The fluoride compound most often added to fluxes is CaF_2. The flux basicity index (BI) most often used in the literature, namely Tuliani's BI, is also expressed in terms of CaF_2 in Equation (1) [5,6]. An important empirically determined flux composition guideline is to ensure that the BI is formulated to be higher than 1.5 to ensure low total oxygen and hydrogen content in the weld metal [5,6].

$$BI = \frac{[\%CaF_2 + \%CaO + \%MgO + \%BaO + \%SrO + \%Na_2O + \%K_2O + \%Li_2O + 0.5(\%MnO + \%FeO)]}{[\%SiO_2 + 0.5(\%Al_2O_3 + \%TiO_2 + \%ZrO_2)]} \quad (1)$$

It is well illustrated in literature that excess oxygen is added to the weld pool via metal droplets melted in the arc cavity, up to 2000–3000 ppm O [2,7,8]. Due to the high temperatures in the arc plasma, the less stable oxides in the molten flux are partially decomposed into oxygen anions and metal cations. Oxygen is adsorbed onto the surface of the molten weld wire droplets in the arc cavity. Therefore, the flux chemistry is manipulated to control the weld metal oxygen content within the desired bands of application, as illustrated in the empirical trend of 200 to 900 ppm O vs. 0.5 to 3.5 BI from Tuliani's work [6,9]. The stability of oxides in the arc plasma was measured in welding tests made with binary CaF_2-oxide flux mixtures, from high to low stability: CaO, K_2O, Na_2O and TiO_2, Al_2O_3, MgO, SiO_2 and MnO [9]. Thus, by increasing the flux CaF_2 content, the proportion of low stability oxides in the flux, and thus also in the molten flux (slag), is effectively diluted to ensure lower ppm O in the weld metal. Acceptable weld metal impact toughness is ensured by controlling the weld metal oxygen content within a relatively narrow band of 200 to 500 ppm oxygen [10].

Although an excessive quantity of 2000–3000 ppm O has been measured in molten weld wire droplets, and this oxygen is carried into the weld pool by the molten weld wire droplets, most of the excess oxygen transferred from the arc cavity reacts with the molten steel at the arc plasma–weld pool interface to form FeO, which is added to the slag. The trend of increased FeO in the slag associated with increased ppm O in the weld metal has been well-reported in several studies [11–16].

It is stated in literature that it is difficult to transfer Al and Ti across the welding arc and into the weld metal [17]. This effect is most likely due to the high oxygen affinity of these metals combined with the highly oxidising conditions prevailing in the arc. In our previous studies on SAW, we applied Al metal powder in combination with the metal powders of the transition metals, Ti and Cr, respectively. The Al powder controlled the oxygen potential at the flux–weld pool interface to ensure increased Ti or Cr metal powder transfer into the weld metal and maintain acceptable levels of ppm O in the weld metal [18,19].

The application of unconstrained metal powders (not fluxed cored wire or metal cored wire) in SAW has been applied before to increase welding productivity in welding joint applications by adding Fe powders and in cladding applications by using a mixture of Fe and alloy powders [20–22]. Limited published studies have reported on the application of unconstrained metal powders to form highly alloyed weld metal in SAW. Knowledge of the behaviour of the different alloying elements, and their interaction with each other and with oxygen, will guide optimal process development choices to attain efficient alloying from the metal powders. This is especially important in the application of high oxygen affinity elements such as Al, Ti, and Cr.

The ability to alloy the weld metal with metals of high oxygen affinity is important for the application of SAW to low density/high-entropy steels. From the concept of high-entropy alloys (HEAs) and compositionally complex alloys (CCAs), the development of low density/high-entropy steels has emerged [23]. The developmental aim of low density/high-entropy steels is to improve steel material properties, namely tensile strength and ductility, simultaneously. By making high alloy additions to Fe, the play-off between steel tensile strength and ductility is bypassed as both properties are improved at the same time, as in the case for HEAs [23]. More recently, this concept has been expanded to develop low density stainless steels by adding Al together with Cr and Mn [24]. Therefore, a method of welding highly alloyed plates of low density/high-entropy steels to form a matched weld metal joint is an important developmental target in utilising low density steels in manufacturing. Because SAW is a high production productivity welding process, the extension of SAW application to a wide class of newly developed steels, such as low density/high-entropy steels, will benefit the engineering industry.

The method of alloying the weld metal to the desired composition must be matched to the specific alloying element's chemical behaviour and the interaction between the selected alloying elements. For example, the addition of Al via weld wire is unlikely to be a workable method due to the high affinity of Al for oxygen. Aluminium is an important alloying element specifically used in low density/high-entropy steels for its lower density and low mixing enthalpy with most other alloying elements [24,25]. Although low density/high-entropy steel development is in its infancy and is centred on Fe-C-Mn-Al-Si steel formulations, different alloying additions are under investigation [24,25].

Increased levels of copper are used in carbon steels. For example, 4% Cu is applied in chrome–manganese stainless steels to improve steel corrosion resistance and maintain good weldability [26]. Alloying of the weld metal with Cu is complicated as it causes weld wire work hardening, which means the weld wire is not easily drawn to the required diameter and the weld wire is also not easily fed through the feeding rollers of the welding equipment [27]. Therefore, alloying of the weld metal in SAW with larger quantities of Cu may be more easily accomplished if copper is added as metal powder. Titanium is added in small quantities to stainless steels to prevent sensitisation to intergranular corrosion [28]. The addition of higher quantities of Ti with Cr may open up new applications for the use of higher Ti alloying of low density stainless steels. However, stainless steels containing Al and Ti can only be arc welded with gas-shielded processes [28]. In our previous work, we demonstrated the alloying of carbon steel weld metal in SAW via unconstrained metal powders of Ti and Al, Cr and Al, and Ti-Cu-Al, respectively [18,19,29]. Here, we add Cr metal powder to the Ti-Cu-Al powder, for the same initial Al quantity, to demonstrate the incorporation of Cr metal powder under oxygen potential control at the molten flux–weld pool interface.

From the above discussion, it is clear that weld metal alloying by elements of high oxygen affinity is an important prerequisite in the process application of SAW to low density/high-entropy steels. The purpose of this work is to illustrate the application of unconstrained Al-Cu-Ti-Cr metal powder addition in SAW to stabilise metal powder uptake into the weld metal and control the ppm O in the weld metal within the target of 200–500 ppm O.

2. Experimental Section

As a comparative base case (BC), one of the welding experiments was made without adding any metal powders. Two welding experiments were made with the addition of metal powders of different mixtures, namely MP3 with Al-Ti-Cu metal powders and MP5 with Al-Ti-Cu-Cr metal powders added. The results from the weld runs with alloy metal powders illustrate the process concept of sufficient oxygen potential control at the molten flux–weld pool interface to improve metal powder alloying into the weld pool.

The SAW experiments consisted of bead-on-plate welds onto steel plates of dimensions 350 mm length, 12 mm plate thickness, 300 mm plate width. A generally used structural steel grade, EN 10025-2, of composition in Table 1 was used as base plate material. The weld heat input was kept constant at 2.0 kJ/mm by using weld parameters set to 500 A, 28 V and 42 cm/min welding speed at Direct Current Electrode Positive (DCEP). Solid weld wire of 3.2 mm diameter was used. The weld wire composition is shown in Table 1. The weld wire composition is taken from the supplier's specification sheet, namely Afrox Ltd., Johannesburg, South Africa. The base plate steel was analysed with an optical emission spectroscopy (OES) instrument from SPECTRO Analytical Instruments GmbH, model SpectroMax XF, 2018. The oxygen content in the base plate and weld wire was analysed by combustion method.

Each welded plate was sectioned across the weld bead at three different positions along the plate length, close to the centre of the weld run, to remove three cross-section samples of the weld metal. Analysis methods included OES of the major elements and the combustion method for total oxygen content analyses. Because the concentration levels of Ti and Al in the weld metal were in excess of the levels in typical carbon steel standards, these elements

were analysed by ICP-OES (inductively coupled plasma optical emission spectrometry) instead of OES. SEM micrographs and analyses of the weld metal were obtained by using a Zeiss crossbeam 540 field emission gun (FEG) scanning electron microscope (SEM). The energy dispersive spectrometer (EDS) analyses were done at 20 kV and 5.6 mm working distance using an Oxford Aztec system with X-Max 80 detector. SEM-EDS equipment model is of the year 2015.

Table 1. Steel base plate and weld wire compositions (mass%).

	%C	%Si	%Mn	* O	%Al	%P	%S	%Ti	%Cu	%Cr	Balance
Plate	0.120	0.155	1.340	7	0.067	0.019	0.007	0.005	0.030	0.160	Fe
Wire	0.110	0.137	0.990	3	0	0.009	0.023	0	0.140	0	Fe

* ppm.

Following a study of the welding process characteristics of various commercial agglomerated fluxes, the Aluminate Basic flux (Basicity Index (BI) = 1.4) of composition in Table 2 was selected for this work [30]. Pure metal powders were used, namely Al (99.7% Al) from Sigma–Aldrich (St. Louis, MO, USA), Ti (99.5% Ti) from PLS Technik GmbH & Co. (Sassenburg, Germany), Cu (99.8% Cu) from Goodfellow, and Cr (99.0% Cr) from Alfa Aesar.

Table 2. Flux bulk chemical composition (mass%).

MnO	CaO	SiO_2	Al_2O_3	CaF_2	MgO	FeO	TiO_2	Na_2O	K_2O
6.8	0.1	19.6	24.9	17.9	22.2	2.4	1.0	1.6	0.2

3. Results

The weld metal compositions of three scenarios are summarised in Table 3. The balance of each weld metal composition in Table 3 is Fe. In the first scenario, namely the Base Case (BC), zero metal powder was added in the welding process. In the second scenario, equal mass quantities of Al, Ti, and Cu metal powders were added in the welding process to form MP3 weld metal. In the third scenario, equal mass quantities of Al, Ti, Cu, and Cr metal powder were added in the welding process to form MP5 weld metal. Each metal powder mass quantity was set to 10 g.

Table 3. Weld metal compositions (mass%).

	%C	%Si	%Mn	* O	%Al	%P	%S	%Ti	%Cu	%Cr
Base Case	0.110	0.260	1.300	499	0.032	0.022	0.011	0.005	0.110	0.110
MP3	0.074	1.040	1.640	371	5.257	0.015	0.012	5.113	3.587	0.167
MP5	0.092	1.250	1.470	326	4.843	0.021	0.014	5.887	4.953	5.923

* ppm.

The comparison of the weld metal analyses displayed in Table 3 confirms alloying of the MP weld metals through the added Si, Mn, Al, Ti, and Cu and alloying of the MP5 weld metal with Cr. Thus, the alloying effect of the added metal powders in SAW is clearly demonstrated. The ppm O in the MP3 and MP5 welds are close in magnitude, at 371 ppm and 326 ppm O, compared to the higher value of 499 ppm O in the BC weld metal. This effect is expected because Al powder serves as a deoxidiser element at the weld pool–molten flux interface [18].

As a check of the bulk chemistry analyses in Table 3, EDS analyses of selected areas in the MP5 weld metal micrograph in Figure 1 were made. Similar EDS analyses in the MP3 weld metal have been described previously [29]. These EDS analyses in Table 4 confirm that

alloying of MP5 weld metal was achieved, in agreement with the bulk chemistry analysis in Table 3. The increased levels of Si and Mn analysed in the weld metal of both the MP3 and MP5 welds (see Table 3) confirm that MnO and SiO_2 were reduced by Al powder, in accordance with reactions (2) and (3). The reaction enthalpy change at 2000 °C (2273 K) for each reaction is shown next to the reactions, (2) to (4). Because FeO is also typically formed in the SAW molten flux, it is likely that some of this FeO was reduced by Al according to reaction (4). The exothermic reaction enthalpy from reactions (2) and (3) is quantified in Section 4.3.

$$3(SiO_2) + 4(Al) = 3(Si) + 2(Al_2O_3) \;\; \Delta H_{2273} = -82.1 \text{ kJ/mol Al} \quad (2)$$

$$3(MnO) + 2(Al) = 3(Mn) + (Al_2O_3) \;\; \Delta H_{2273} = -248.4 \text{ kJ/mol Al} \quad (3)$$

$$3(FeO) + 2(Al) = 3(Fe) + (Al_2O_3) \;\; \Delta H_{2273} = -416.5 \text{ kJ/mol Al} \quad (4)$$

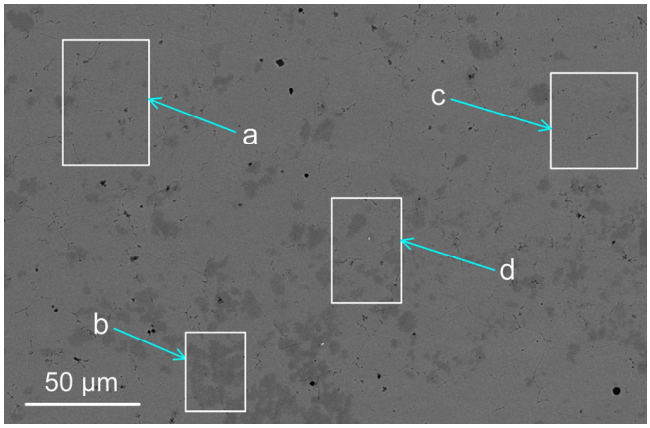

Figure 1. SEM micrograph of MP5 weld metal analysed areas (×1010).

Table 4. SEM-EDS analyses of marked areas in Figure 1 (mass%).

	%Si	%Mn	%Al	%Ti	%Fe	%Cu	%Cr
a	0.83	1.39	3.78	5.26	77.8	5.20	5.70
b	0.89	1.39	3.51	4.93	78.6	5.09	5.61
c	0.87	1.58	3.52	4.58	79.1	4.83	5.54
d	0.89	1.47	3.67	5.33	77.9	5.09	5.65

Even though the Al reduction reactions with SiO_2 and MnO are thermodynamically favoured, sufficient contact time between the added Al powder and the molten flux is required to ensure that reactions (2) and (3) proceed sufficiently to alloy the weld metal. Increased Si and Mn analyses values in MP3 and MP5 weld metals, compared to the BC values, confirm that sufficient contact time was available for reactions (2) and (3) to proceed to a significant extent. Because reactions (2) and (3) occurred at the molten flux–weld pool interface, the Al_2O_3 products from these reactions should easily absorb into the molten flux. Furthermore, the application of Al powder to maintain sufficiently reducing conditions at the molten flux–weld pool interface ensures that most of the added Ti and Cr powder is added into the weld pool. In the absence of Al powder, the excess oxygen in the weld metal reacts with the Ti and Cr metal powders and forms Ti-oxides and Cr-oxides, thus preventing alloying of the weld pool. Very little of the weld metal Ti and Cr is present as oxides because the weld metal ppm O quantities in the MP3 and MP5 weld metal analyses are too small in proportion to the weld metal %Ti and %Cr to convert much of the weld metal Ti and Cr to oxides. Thus, limited quantities of Ti and Cr powders appear to be wasted on oxygen reactions to form Ti and Cr oxides in the weld metal. This is most likely

because oxide inclusion formation preference is set by the thermodynamic favourability of reactions between the weld pool alloying elements of Al, Ti, Cr, Si, Mn, and oxygen, indicating a preference for Al_2O_3 to form first.

Mass balance calculations were applied to calculate the grams of Al, Ti, Cr, and Cu added into MP3 and MP5 weld metal. The calculation procedure is described in the following section, and the mass values are reported in Table 5. From each welding test, the mass of metal added to the welded plate was calculated from the difference between the post-weld plate mass and the pre-weld plate mass. For each weld run, the weld metal cross-section polished section was etched with 2% Nital solution to reveal the weld metal boundary in the base plate. The etched weld metal cross-section was then used to measure the weld metal areas above and below the base plate level. Area measurements were made from the stereoscope image of each weld metal cross-section by applying the stereoscope supplier's computer software. This method is similar to the literature-reported method used in bead-on-plate SAW [31]. The method, as applied here, is the same as in our similar previous works, namely in that the area above the base plate level represents the mass proportion contribution of weld wire and metal powder to the total weld metal mass [29,32]. This mass proportion contribution ratio is defined as the dilution ratio percentage ($\%DR_{(wire+MP)}$) and is expressed in Equation (5). The mass of Al, Ti, Cr, and Cu added to the weld metal was calculated from Equations (5)–(7). The weld metal composition in Table 3 was used as an input to Equation (7). Here, Equation (7) is displayed to illustrate the calculation of the mass of Al added to the weld metal. Similar calculations were made for the Ti, Cr, and Cu mass added to the weld metal by using the weld metal composition %Ti, %Cr, and %Cu in Table 3 as respective inputs to Equation (7).

$$\%\mathrm{DR}_{(\mathrm{wire+MP})} = \left(\frac{\mathrm{A}_{(\mathrm{wire+MP})}}{\mathrm{A}_{(\mathrm{wire+MP})} + \mathrm{A}_{\mathrm{BP}}}\right) * 100 \quad (5)$$

$$\mathrm{m}_{\mathrm{WM}} = (\mathrm{m}_{\mathrm{wire}} + \mathrm{m}_{\mathrm{MP}}) * \left(\frac{100}{\%\mathrm{DR}_{(\mathrm{wire+MP})}}\right) \quad (6)$$

$$(\text{gram Al to WM}) = (\mathrm{m}_{\mathrm{WM}}) * \left(\frac{\%\mathrm{Al}_{\mathrm{WM}}}{100}\right) \quad (7)$$

WM = weld metal; MP = metal powder; BP = base plate; Wire = weld wire; m = mass (gram); A = area (mm^2)

Table 5. Post-weld masses and metal powder mass added to weld metal.

	Al (g)	Ti (g)	Cu (g)	Cr (g)	* Powder (g)	Wire (g)	Base Plate(g)	Weld Metal (g)	Slag (g)	$\%DR_{(wire+MP)}$
Base Case	0	0	0	0	0	33.8	33.8	67.6	65.9	50
MP3	4.8	4.7	3.3	0	12.8	54.7	23.7	91	42.9	74
MP5	5.2	6.4	5.4	6.4	23.4	56.6	28.1	108	36.4	74

* Total of Al, Ti, Cu, and Cr powder added into the weld metal.

The grams of Al, Ti, Cr, and Cu added into weld metal are summarised in Table 5. The grams of the total weld metal formed, the grams of base plate melted into the weld and the mass of weld wire melted into the weld, and the mass of slag melted from the flux, are also summarised in Table 5. It is seen from the data in Table 5 that higher mass quantities of Al, Ti, and Cu were incorporated into MP5 weld metal in comparison to MP3 weld metal alloying additions. Although the mass of the weld wire added into MP3 and MP5 weld metal are similar and the ($\%DR_{(wire+MP)}$) numbers are the same, more metal powder was added in total to MP5 weld metal as compared to MP3 weld metal.

The percentage yield of each alloying element from 10 g of each element added is displayed in Table 6. Similarly, the total metal powder yield values from the total of 30 g added to the MP3 weld run and total of 40 g added to MP5 weld run are also displayed

in Table 6. It is seen that more metal powder was melted into the MP5 weld pool and somewhat less slag was melted compared to the MP3 values. Compared to the base case, much less slag was melted in the MP3 and MP5 tests, indicating a reallocation of heat to the melting of the metal powders instead of melting the flux to slag. To better explain the difference in the total metal powder incorporation between MP3 and MP5 weld metals, the chemical interaction between the alloying elements should be considered, as set out in Section 4.

Table 6. Metal powder yield information as mass%.

	Al (g)	Ti (g)	Cu (g)	Cr (g)	* Powder (g)	%Al Yield	%Ti Yield	%Cu Yield	%Cr Yield	%Powder Yield
MP3	4.8	4.7	3.3	0	12.8	48	47	33	0	43
MP5	5.2	6.4	5.4	6.4	23.4	52	64	54	64	59

* Total of Al, Ti, Cu, and Cr powder added into the weld metal.

4. Discussion

4.1. Alloy Melt Formation and Chemistry

The liquidus temperature of the pure alloying elements Al, Cu, Ti, and Cr are 660 °C, 1083 °C, 1660, and 1857 °C. It is expected that the incorporation of these alloying elements into the weld pool is sequenced according to the liquidus temperature of the elements. Therefore, the melting sequence is expected to be firstly Al, then Cu, then Ti, and lastly Cr. Binary and multi-element phase diagram information is applied in the following discussion to delineate the chemical interaction of the alloying elements and their chemical interactions with Fe.

Binary alloy phase diagrams, available in the literature, are displayed in Figures 2–6 and illustrate the chemical interactions among the main elements in the weld pool [33]. As shown previously for MP3 weld metal, Cu and Ti may interact chemically to form an initial low temperature melt, as indicated in Figure 2 [29]. The stabilising effect of Cu in the MP3 weld pool is due to its extensive lowering of the Ti liquidus temperature from 1660 °C to as low as 992 °C at the mol ratio of Ti/(Cu + Ti) = 0.65 at the red arrow in Figure 2. The proportional composition of Ti and Cu in the MP5 weld pool is at the mol ratio of Ti/(Cu + Ti) = 0.61, similar to that in MP3, as indicated by the green arrow in Figure 2. Therefore, if only Figure 2 is considered, the chemical effect of the Cu alloying of the weld pool is similar for MP3 and MP5 because the weld metal proportional compositions from Table 3 may form Cu-Ti melts of a significantly lower liquidus temperature than pure Ti.

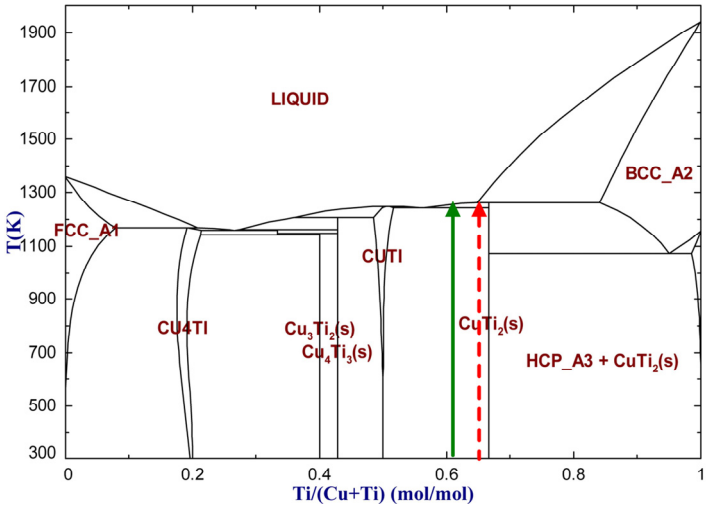

Figure 2. Binary phase diagram of Cu and Ti from FactSage 7.3 databases [33].

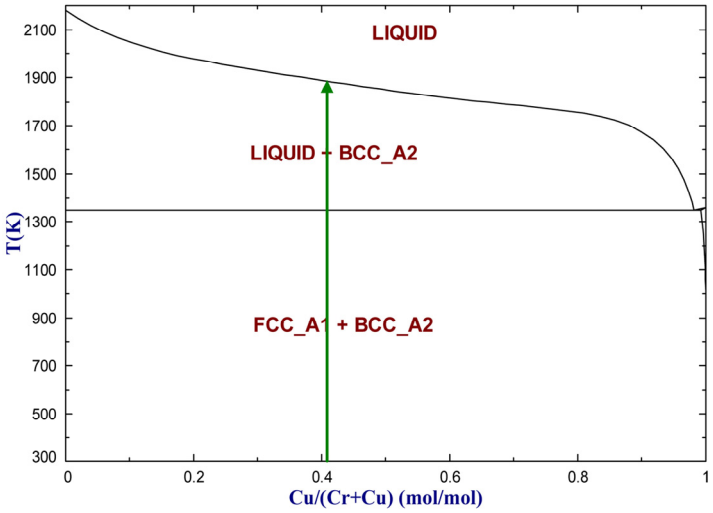

Figure 3. Binary phase diagram of Cr and Cu from FactSage 7.3 databases [33].

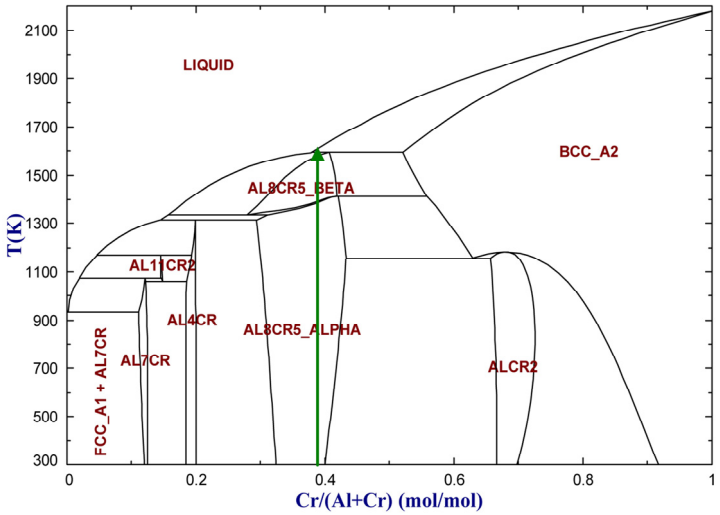

Figure 4. Binary phase diagram of Cr and Al from FactSage 7.3 databases [33].

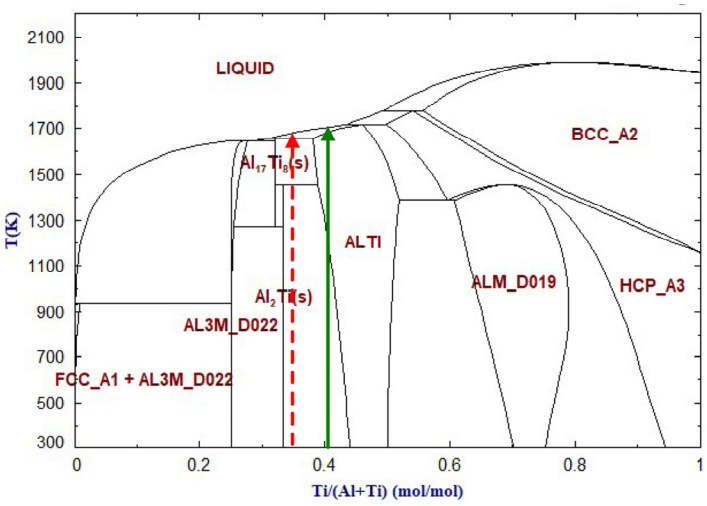

Figure 5. Binary phase diagram of Ti and Al from FactSage 7.3 databases [33].

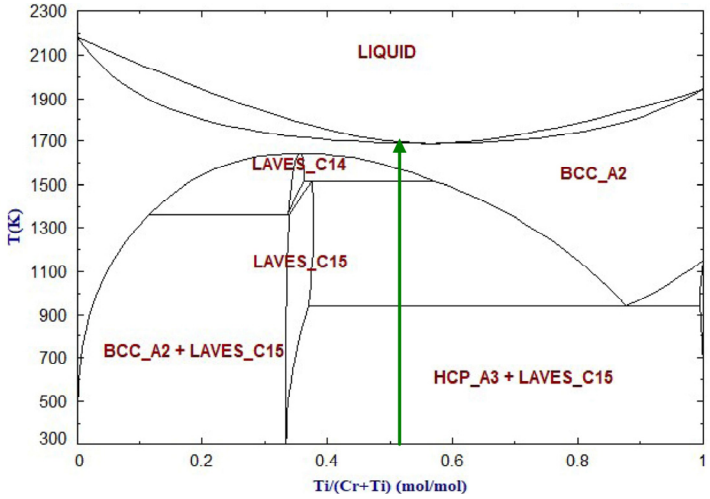

Figure 6. Ti-Cr phase diagram from FactSage 7.3 databases [33].

The Cu-Fe and Cu-Al phase diagrams are not shown here since Cu has only a slight liquidus lowering effect when added to pure Fe or pure Al at the proportions displayed in Table 3. The effect of Cu in lowering the liquidus temperature of Cr should also be considered, as is shown in Figure 3. It is seen that Cu also has a stabilising effect on Cr, similar to its effect on Ti, since it lowers the Cr liquidus temperature from 1857 °C to 1627 °C at the mol ratio of Cu/(Cr + Cu) = 0.41 (see the green arrow in Figure 3). However, the effect of Al in lowering the Cr liquidus temperature is larger than the effect of Cu in lowering the liquidus temperature of Cr, as indicated in Figure 4, with a mol ratio of Cr/(Al + Cr) = 0.39. The Cr liquidus temperature is lowered by 530 °C from 1857 °C to 1327 °C at the proportional Cr-Al composition in Figure 4. In contrast, the liquidus lowering effect of Al on Ti is less than that of Cu on Ti, as shown in Figure 5 for MP3 at the red arrow and for MP5 at the green arrow. However, based on the liquidus temperatures of the pure elements, one would expect the incorporation sequence to consist of the initial formation of an Al-Cu alloy, followed by melting of Ti and Cr into this alloy. Therefore, the relevance of Figures 4 and 5 in MP5 weld pool chemistry is expected to be limited.

Consideration of the binary phase diagram of Ti-Cr in Figure 6 shows that Cr and Ti are mutually soluble over the whole concentration range. For the proportional composition of Ti and Cr in MP5 weld metal from Table 3 at mol ratio Ti/(Cr + Ti) = 0.52, the maximum mutual liquidus temperature lowering effect is achieved to 1427 °C. Therefore, this liquidus lowering effect is 430 °C for pure Cr by lowering the pure Cr liquidus temperature to 1427 °C and lowering the liquidus temperature of pure Ti by 233 °C to 1427 °C. Consideration of the Cr-Ti binary phase diagram is only indicative of the effects expected in the multi-component alloy system, as the initial melt is formed from the alloying metal powders and not from Cr and Ti only. As displayed in Figure 2, the lowest initial binary melt from the metal powders appears to be of a similar composition, and is fully molten at 992 °C in the Ti-Cu binary system for both MP3 and MP5 weld metal chemistry (see Figure 2). Therefore, the Ti-Cu-Al vs. Ti-Cu-Al-Cr phase diagrams are considered in Figures 7 and 8 for 1300 °C to illustrate the likely alloy melt formation sequence following the initial Ti-Cu alloy melt formation. The phase diagram module of FactSage 7.3, using the SGTE alloy database, was used to construct these phase diagrams [33].

It is seen that, in Figures 7 and 8, the initial alloy compositions are fully molten at 1300 °C at the filled triangle composition points. As is shown in Figure 8, even though pure Cr has a high liquidus temperature, the incorporation of Cr at up to 27% in the Ti-Cu-Al melt forms a molten melt at the relatively low temperature of 1300 °C, as the Ti-Al intermetallic phase areas displayed in the Ti-Cu-Al phase diagram is replaced by BCC and liquid phase areas.

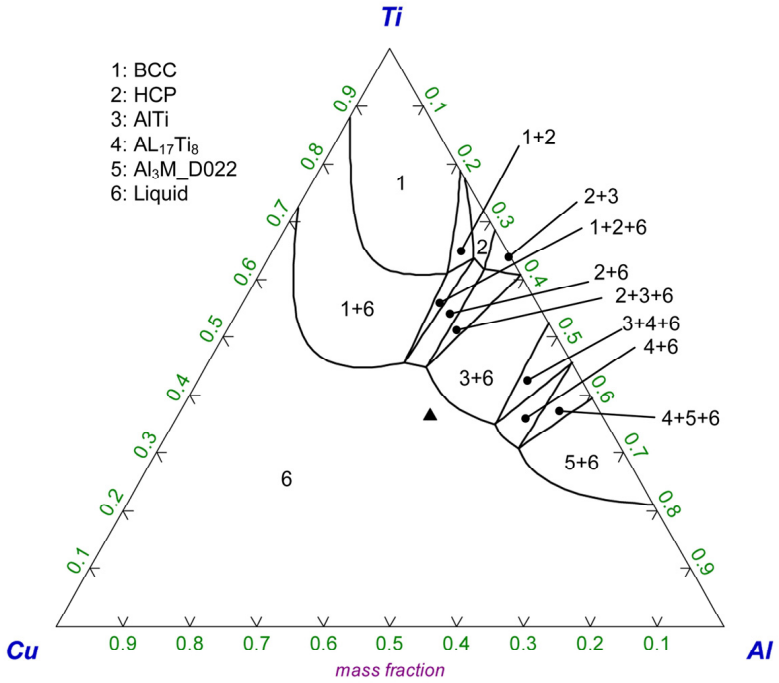

Figure 7. MP3 initial alloy (filled triangle) in Cu-Al-Ti phase diagram for 1300 °C as calculated in FactSage 7.3 [33].

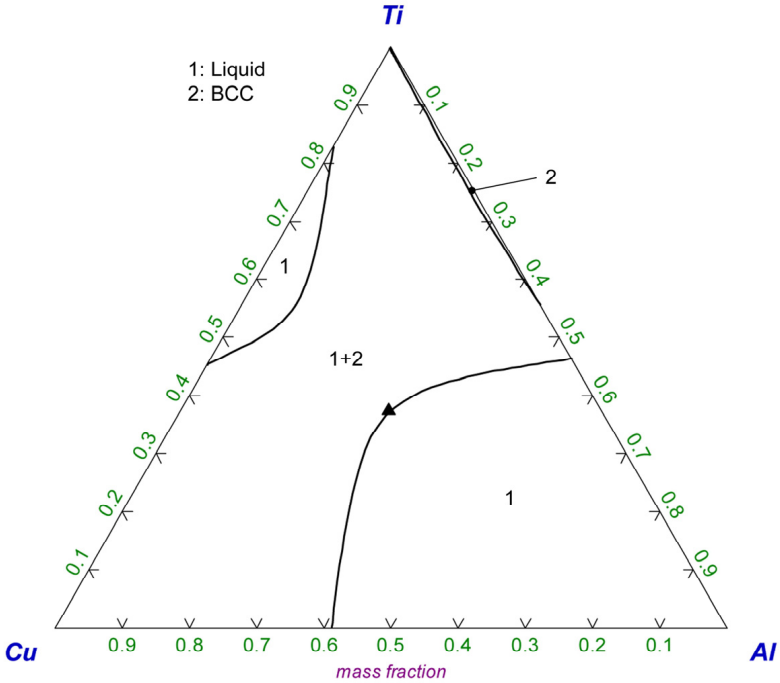

Figure 8. MP5 initial alloy (filled triangle) in Cu-Al-Ti-27% Cr pseudo ternary phase diagram for 1300 °C as calculated in FactSage 7.3 [33].

4.2. Weld Pool Chemistry Evolution

Following the initial melt phase formation from the metal powders, mixing of molten weld wire, base plate, and the initial melt takes place. Figure 9a–d illustrates the phase chemistry results of increased Fe added into the starting alloy melt phase in MP5 weld metal formation, shown in Figure 8. The relevant composition points are indicated as filled triangles in Figure 9a–d. Iron added into the initial Ti-Cu-Al-Cr alloy melt results in a shift in phase fields. The BCC + liquid phase field in Figure 8 is dissected, and this results in the

joining of the two liquid phase fields in Figure 8 to form one continuous liquid phase field across all Al contents, as displayed in Figure 9a–c. The phase diagrams in Figure 9 illustrate that Fe uptake into the initial Cu-Al-Ti-Cr melt can be accommodated up to 60% Fe and still maintain 100% liquid at 1300 °C (see Figure 9d). Adding more Fe to attain the final steel composition at 78% Fe in a 100% liquid melt would require 1400 °C. Even though the weld pool formation and solidification in SAW spans only a few seconds, the phase diagrams in Figures 8 and 9 illustrate that the sequence of alloying from the low temperature alloy melt of Cu-Al-Ti-Cr to the final steel composition is completed in this short time. Further exploration of the effect of alloying on weld pool chemistry is shown as liquid proportion vs. temperature curves for each weld metal composition, as illustrated in Figure 10. The phase chemistry curves displayed in Figure 10 were calculated in FactSage 7.3 by using the FToxid and FSstel databases in the Equilib module of the software [33].

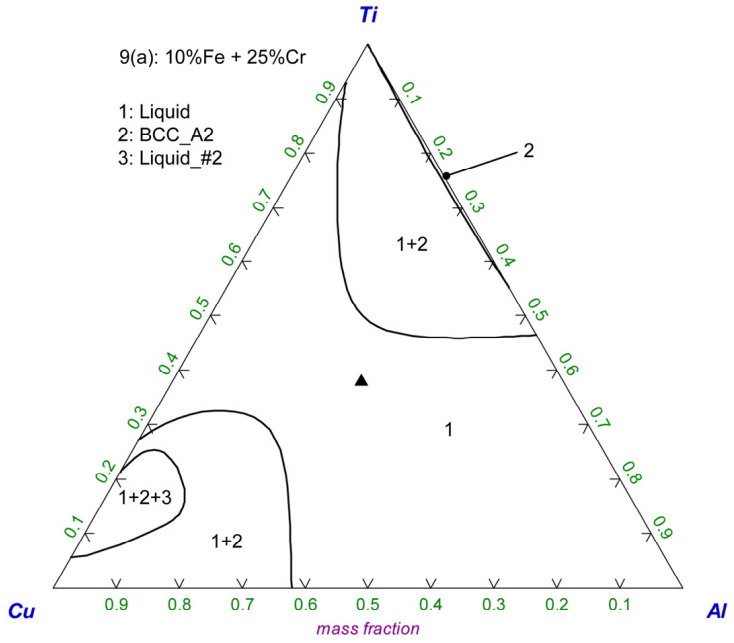

Figure 9. *Cont.*

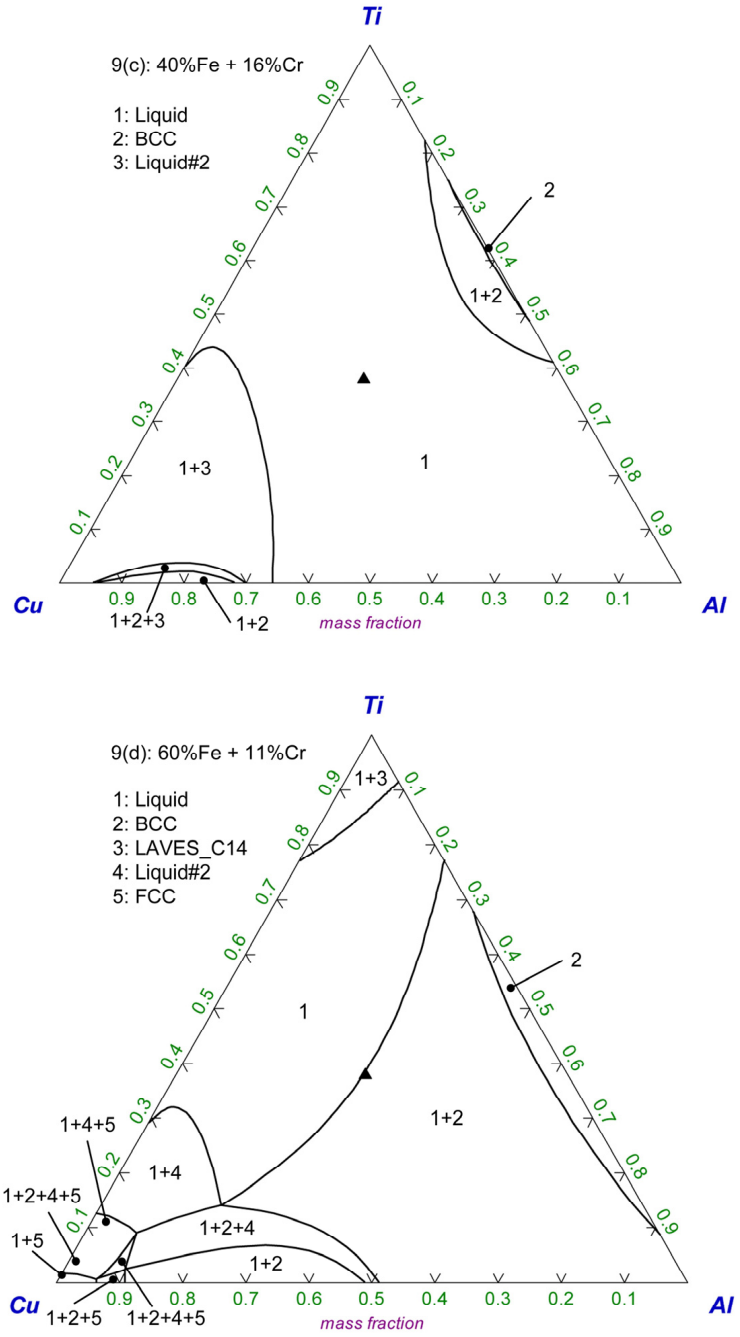

Figure 9. (**a**–**d**) Cu-Al-Ti-Cr-Fe pseudo ternary phase diagrams for 1300 °C at increased %Fe, as calculated in FactSage 7.3 [33].

The proportion liquid alloy at increased %Fe added into the initial alloy melt compositions for MP3 and MP5 welds from Figures 7 and 8 are illustrated in Figure 10a–f. It is seen that the liquid alloy proportions are higher in the MP3 weld pool at 5% Fe to 30% Fe. However, at 60% Fe to 75% Fe, the MP5 weld pool chemistry contains more liquid alloy at the same temperature. Drastic differences in solidus temperature are displayed between MP3 and MP5 weld pool chemistries at 60% Fe and 70% Fe. For example, at 70% Fe and 1300 °C, the MP3 weld pool is completely solidified, compared to the 47% liquid alloy present in the MP5 weld pool. The higher liquid proportions in the MP5 weld pool chemistries at higher %Fe, compared to that in the MP3 weld pool at the same temperature, should contribute to the higher total metal powder incorporated into the MP5 weld metal.

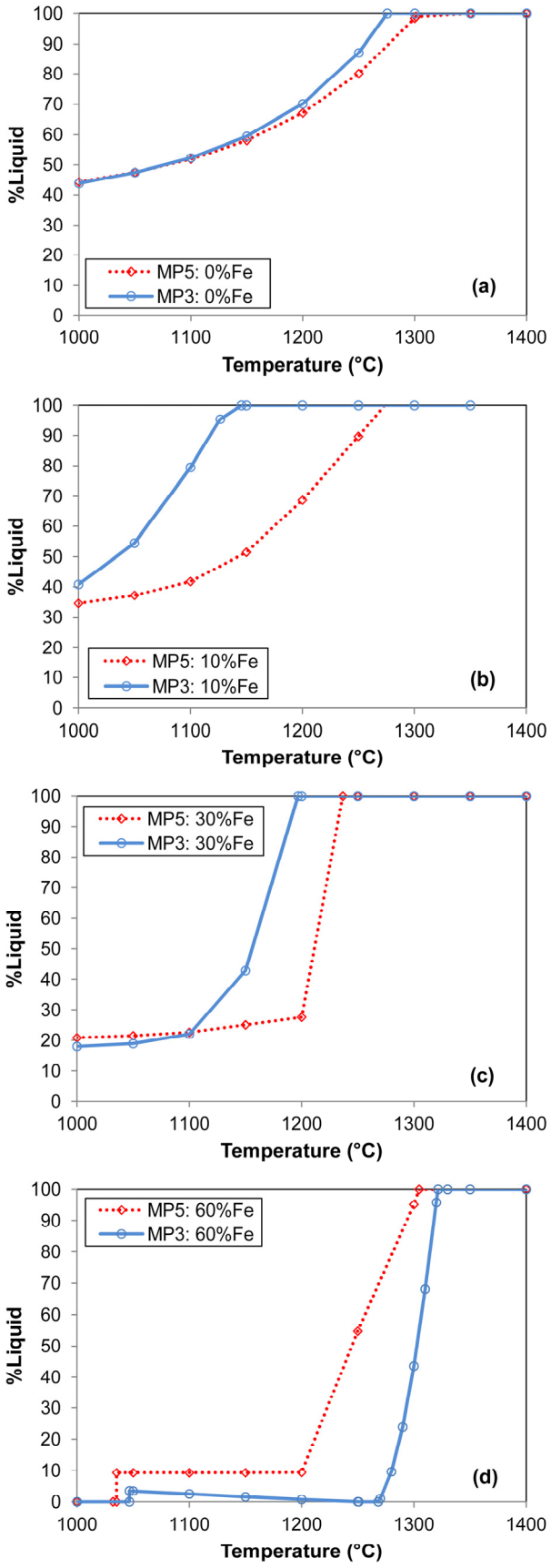

Figure 10. *Cont.*

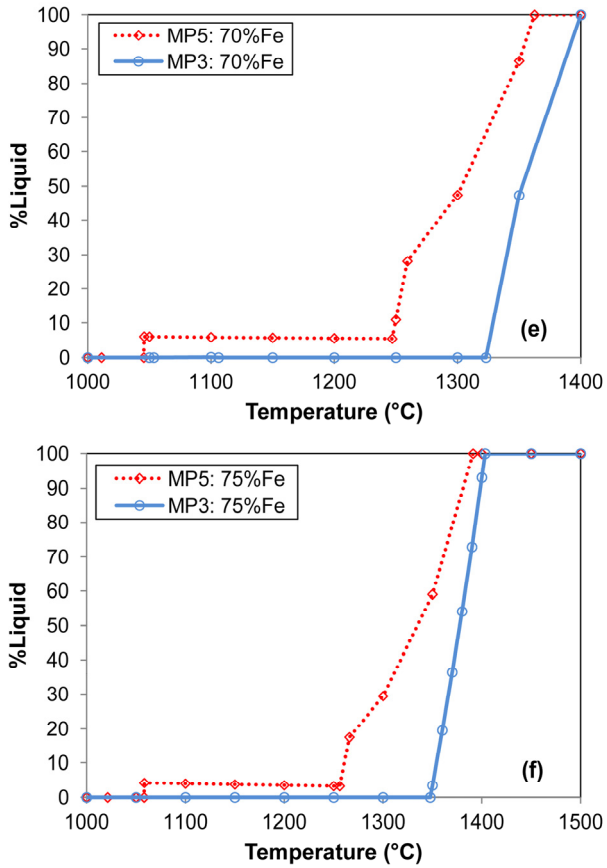

Figure 10. (**a**–**f**) Liquid alloy proportions in Cu-Al-Ti-Cr-Fe alloy at increased %Fe, as calculated in FactSage 7.3 [33].

4.3. Exothermic Heat of Al Reactions

The exothermic reactions (2) and (3) occurred to a significant extent, as evidenced by the increased analyses of weld metal Mn and Si contents in MP3 and MP5 (see Table 3) in comparison with the Mn and Si contents in the BC weld metal. It is important to quantify the heat added to the weld pool from these reactions to investigate if there are differences in the exothermic heat generated in the MP3 and MP5 weld pool, as this is extra heat may aid in weld pool formation. Therefore, the grams of Mn and Si added to the MP weld metals, relative to the BC weld metal nominal composition, were calculated in order to quantify the extent of the exothermic reduction reactions of MnO and SiO_2 by Al (reactions (2) and (3)). The calculations are made via Equation (8), as reported previously [29]. Inputs to Equation (8) to calculate the mass of the Mn added were derived from the input values of the weld metal mass (M_{MN}) and the dilution ratio value ($(\%DR_{(wire+MP)}$) from Table 5. To calculate the mass of Si added to the weld metal, relative to the mass of Si added to the BC weld metal, the %Si values are used as inputs in Equation (8), instead of the %Mn values, as reported previously [29]. The square bracketed terms in Equation (8) represent the calculation of the BC weld metal nominal composition.

$$m_{Mn} = (m_{WM})\left(\frac{\%Mn_{WM}}{100} - \left[\frac{\%DR_{wire}}{100} * \frac{\%Mn_{wire}}{100}\right] - \left[\left(1 - \frac{\%DR_{wire}}{100}\right) * \frac{\%Mn_{BP}}{100}\right]\right) \quad (8)$$

M = mass (gram); M_{MN} = mass Mn (gram); $\%Mn_{WM}$ = %Mn in weld metal; %DRwire = % of weld metal contributed by weld wire in the Base Case (BC); %Mnwire = %Mn in weld wire; $\%Mn_{BP}$ = %Mn in Base Plate (BP); WM = weld metal; BP = base plate; Wire = weld wire

Table 7 shows the calculation results in terms of the mass of SiO_2 and MnO reduced from the slag by Al powder via reactions (2) and (3). These values are conversions of the

mass values of Mn and Si calculated from Equation (8), since the grams of Mn and Si are expressed as the oxide masses, grams of MnO, and grams of SiO_2 in Table 7. The heat generated from each reduction reaction, as calculated from the exothermic reaction enthalpy values at 2273 K ($\Delta H_{2273\,K}$) displayed next to reactions (2) and (3), are also summarised in Table 7 as kJ values. The heat capacity of steel (0.460 kJ/kg K) was used to translate the total exothermic heat values of −4.5 kJ and −5.6 kJ to its heating effect in increased weld pool temperature. Since the exothermic heat values for MP3 and MP5 weld metal are similar, at −4.5 kJ and −5.6 kJ exothermic heat evolved, the translated values of weld metal heating are also similar at 107 °C and 113 °C, respectively. These values are likely minimum values because the extent of reaction (4) is not known, even though reaction (4) definitely proceeded in part, since it is used to control the partial oxygen pressure at the weld pool–slag interface [18]. Because the same welding parameters and the same welding flux were used in all the welding tests, it is expected that the same quantity of oxygen was transferred from the arc cavity, via the molten weld wire droplets, into the weld pool. Therefore, the extent of FeO formation and FeO reduction via reaction (4) should be similar in MP3 and MP5 weld metal formation.

Table 7. Exothermic heat from aluminium reduction reactions (2) and (3).

	SiO_2 (g)	MnO (g)	Al (g)	Reaction (2) (kJ)	Reaction (3) (kJ)	Reactions (2) & (3) (kJ)	Weld Metal ΔT (°C)
MP3	1.7	0.6	1.2	−3.2	−1.3	−4.5	107
MP5	2.6	0.4	1.6	−4.7	−1.0	−5.6	113

The important conclusion from the similarity in values for MP3 and MP5 in Table 7 is that the difference in the melting rate of metal powders into MP3 and MP5 weld metal (see Tables 5 and 6) is not explained by the different extents of the exothermic reactions of Al/SiO_2 and/or Al/MnO, as displayed in reactions (2) and (3).

4.4. Weld Metal Solidification Curves

The weld pool solidification time is set by the weld heat input (2.0 kJ/mm) [34]. Here, the same weld heat input was applied in all three welding tests. However, the weld pool chemistries are different, and therefore the liquidus and solidus temperatures of the weld metal compositions in Table 3 are different. The solidification curves in Figure 11 illustrate the effect of alloying in lowering the liquidus temperature from BC to MP3 weld metal, and to a lesser extent from MP3 to MP5 weld metal. Stark differences are seen in the solidification profiles of the weld metals since MP3 and MP5 weld metal solidus temperatures are significantly lowered from that of the BC weld metal.

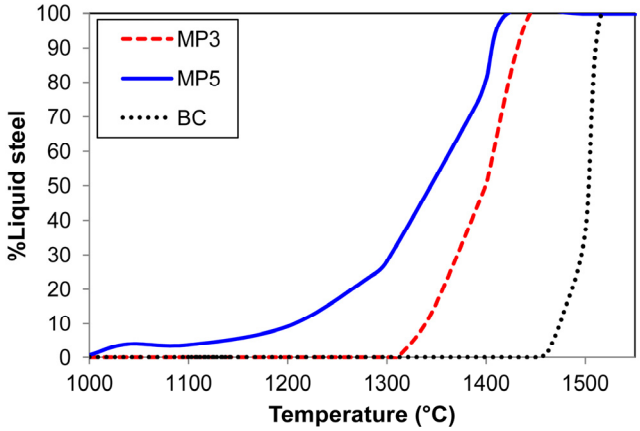

Figure 11. Solidification curves for BC, MP3, and MP5 weld metal compositions calculated in FactSage 7.3 [33].

The lower MP5 weld metal solidus temperature, compared to that of MP3 and the base case (BC) weld metal, results in an increased MP5 weld metal solidification time. This means that more time is available for oxide inclusions to float out of the weld pool liquid steel in the case of MP5 weld metal formation, as compared to the shorter solidification times of the MP3 and BC weld pools. This is important because oxide inclusions must float out to the molten flux–weld pool interface first, and then the oxide inclusions can be removed from the weld pool liquid steel by absorption into the molten flux (slag) [34]. From the similar values of weld metal ppm O in MP3 at 371 ppm O vs. 326 ppm O in MP5, it appears that the longer weld pool solidification time in MP5 weld metal, compared to MP3 weld metal, had a limited effect on the weld metal ppm O. However, a comparison between MP3 and MP5 weld metal ppm O and BC weld metal ppm O at 499 ppm O indicates that weld pool solidification time is an important aspect in setting the total ppm O in the weld metal.

4.5. Improved Productivity in Metal Deposition Rates

It is well-illustrated in the literature that the metal deposition rate, at a set value of welding heat input, is increased when metal powder is added in SAW, in addition to the isolated application of the arc forming solid weld wire [20–22]. This is possible because only 20% of the arc energy is used to melt the weld wire in conventional SAW, namely with the use of solid weld wire [35]. For example, a 50% increase in metal deposition rate was shown in SAW at 500 A, 31 V, 60 cm/min for a two weld wire arrangement (6.3 kg/h) vs. welding with added metal powder in the same two weld wire arrangement (10.4 kg/h) at the same weld heat input settings [22]. Our findings also indicate a significant productivity improvement in metal deposition rates from BC to MP3 to MP5 welds from 5.3 kg/h to 6.3 kg/h to 7.5 kg/h at the same weld heat input (2.0 kJ/mm). These numbers represent percentage increases of 19% for MP3 and 40% for MP5, compared to the BC metal deposition rate. Therefore, it appears that sufficient heat energy is available in the welding process to increase metal deposition rates, provided sufficient process control is applied to ensure weld metal quality, especially weld metal ppm O.

4.6. Reaction Flow of Al Assisted SAW with Metal Al-Cr-Ti-Cu Powders

The initial reaction flow diagram applied previously to explain the role of Al powder in combination with Ti alloying metal powder in SAW is updated, as shown in Figure 12, to include the Al assisted alloying of the weld metal with Al-Cr-Ti-Cu powders [18]. This reaction flow diagram displays the reactions, their reaction sites, and the reaction sequences in the SAW process. The initial part of the diagram (reaction steps A to E1) is drawn based on the accepted understanding of reactions in the SAW process, as described in the published literature [2,7–9,13]. Molten weld wire droplets transfer large quantities of adsorbed oxygen (2000–3000 ppm O) into the weld pool, across the weld pool–arc plasma interface [7,8]. In our work, Al powder is added to the weld pool to control the oxygen potential at the molten flux–weld pool interface by reducing FeO via reaction (4), as displayed in Section 3. This reaction is similar to reaction G in Figure 12. These aluminium reduction reactions are exothermic, and this extra heat is added into the weld pool to further facilitate the melting and dissolution of Ti and Cr.

Despite the added Al, Ti, and Cr powders of high oxygen affinity to the weld pool, the weld metal oxygen content remained relatively high at MP3 at 371 ppm O in MP3 and 326 ppm O in MP5. Because of the low affinity of Cu for oxygen, the Cu metal powder addition does not appear to influence the weld metal oxygen content via chemical reactions. In agreement with our previously reported results, it appears that the weld metal oxygen content is not set by equilibrium deoxidation reactions in the weld pool when significant quantities of Al and Ti metal powders are added to the weld pool [18]. This conclusion is made based on comparison between the weld pool total ppm O and the quantity of dissolved oxygen in literature-reported equilibrium measurements. The total ppm O in the weld metal, captured as inclusions in the solid weld metal, is much higher than the

Al-Al_2O_3 and Ti-Ti_2O_3 deoxidation reaction equilibrium values of 10 ppm O at 0.1% Al and 30 ppm O at 4% Ti in steel at 1600 °C [36]. Similarly, Cr reactions with oxygen do not set the weld metal oxygen content, as the weld metal total ppm O is much higher than the equilibrium-dissolved ppm O of similar chromium-containing alloys with less than 30 ppm O for 1% Al in the alloy at 1600 °C, as taken from the literature [37]. Instead, as discussed previously, the behaviour of Cr at the molten flux–weld pool interface is regulated by reaction (9), similar to reaction G in Figure 12 [19].

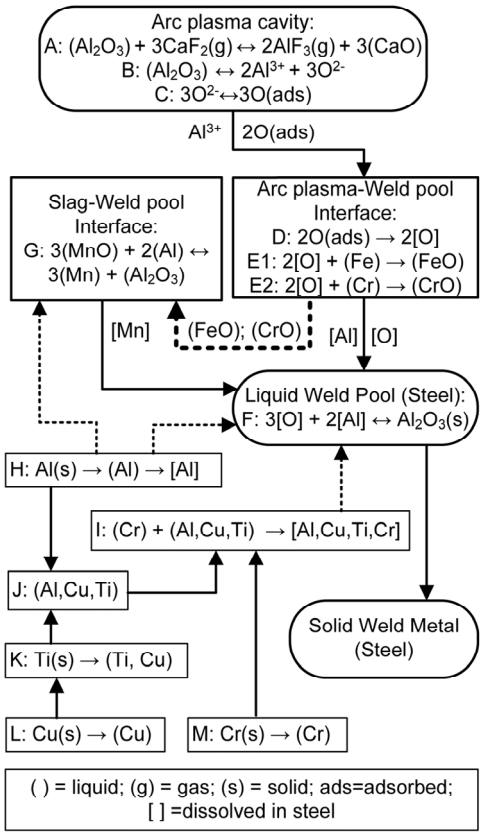

Figure 12. SAW reaction flow diagram with Al, Ti, Cu, and Cr powder addition reactions.

$$3(CrO) + 2(Al) = 3(Cr) + (Al_2O_3) \;\; \Delta H_{2273} = -326.6\ \text{kJ/mol Al} \quad (9)$$

It has been shown that the gas–slag–metal equilibrium applies in SAW in the absence of metal powder additions [11,38]. The same literature-established mechanism of oxygen transfer from the arc cavity to the weld pool appears to hold for the scenarios with metal powder addition, namely MP3 and MP5 [2,7–9,13]. The applicability of the accepted mechanism of the excessively high ppm O of 2000–3000 ppm added into the weld pool from the arc cavity is confirmed by a comparison between the analysed weld metal ppm O values in MP3 and MP5 (371 ppm O and 326 ppm O) and the ppm O values that would set the slag–metal deoxidation reaction equilibria via Al-Al_2O_3 and Ti-Ti_2O_3 in carbon steel and Al-Al_2O_3 in Cr-containing steel, mentioned above at 10 ppm O and 30 ppm O [36,37]. The added Al metal powder ensures that the oxygen potential at the molten flux–weld pool interface is lowered to prevent the oxidation of Ti powder to Ti-oxides and Cr powder to Cr-oxides. Therefore, Ti and Cr metal powders are available to be melted according to the melting sequence of Cu-Ti-Al alloy formation, first with the subsequent incorporation of Cr, as displayed in reaction steps K, J, and I. Any excess Al is dissolved into the weld pool (reaction H). The high oxygen affinity alloying elements dissolved in the weld metal, namely Al, Ti, and Cr, react with oxygen in the steel to form inclusions, similar to reaction F for aluminium. Reactions J and I illustrate the role of Cu as a stabiliser because Cu first

forms a low temperature alloy with Ti and Al, and this alloy effectively decreases the temperature required to melt Cr into the weld pool, via reaction I.

This work confirms that unconstrained Al metal powder can be applied to control the oxygen potential sufficiently at the molten flux–weld pool interface to transfer Ti and Cr metal powder into the weld pool. With this method of oxygen control, the weld metal oxygen ppm O is controlled within acceptable limits. Low temperature melt formation of Cu-Ti-Al incorporates Cr easily.

5. Conclusions

1. This work illustrates that unconstrained Al metal powder additions can be applied to sufficiently control the oxygen potential at the molten flux–weld pool interface to ensure alloying of the weld metal with Ti and Cr;
2. The Al powder addition ensured sufficient control of the oxygen potential at the molten flux–weld pool interface without interfering with oxygen transfer from the arc plasma to the weld pool, resulting in 371 ppm O in MP3 and 326 ppm O in MP5 weld metal vs. 499 ppm O when no metal powder was added;
3. Initial alloy melt formation most likely consisted of the Ti-Cu-Al-Cr in MP5, with subsequent incorporation of Fe;
4. Increased metal deposition rates were confirmed for metal powder addition, compared to no powder addition at the same weld heat input of 2.0 kJ/mm, at 19% increase for MP3 and 40% increase for MP5;
5. Carbon steel alloying to 5.9% Ti, 4.8%Al, 5.0% Cu, and 5.9% Cr was achieved at 326 ppm O.

Author Contributions: F.D.B. conceptualised the work; F.D.B. and T.C. executed the experiments, interpreted the data, and prepared the manuscript. All authors have read and agreed to the published version of the manuscript.

Funding: This research was funded in part by the National Research Foundation of South Africa, grant number BRIC171211293679.

Data Availability Statement: The data sets presented in this study are availabable upon request to the corresponding author.

Conflicts of Interest: The authors declare no conflict of interest. The funders had no role in the design of the study; in the collection, analyses, or interpretation of data; in the writing of the manuscript, or in the decision to publish the results.

References

1. Sengupta, V.; Havrylov, D.; Mendex, P.F. Physical phenomena in the weld zone of submerged arc welding—A Review. *Weld. J.* **2019**, *98*, 283–313.
2. Gött, G.; Gericke, A.; Henkel, K.-M.; Uhrlandt, D. Optical and spectroscopic study of a submerged arc welding cavern. *Weld. J.* **2016**, *95*, 491–499.
3. Chai, C.S.; Eagar, T.W. Slag-metal equilibrium during submerged arc welding. *Metall. Trans. B* **1981**, *12*, 539–547. [CrossRef]
4. Mitra, U.; Eagar, T.W. Slag-metal reactions during welding: Part I. Evaluation and reassessment of existing theories. *Metall. Trans. B* **1991**, *22*, 65–71. [CrossRef]
5. Eagar, T.W. Sources of weld metal oxygen contamination during submerged arc welding. *Weld. J.* **1978**, *57*, 76–80.
6. Tuliani, S.S.; Boniszewski, T.; Eaton, N.F. Notch toughness of commercial submerged arc weld metal. *Weld. Met. Fabr.* **1969**, *37*, 327–339.
7. Polar, A.; Indacochea, J.E.; Blander, M. Electrochemically generated oxygen contamination in submerged arc welding. *Weld. J.* **1990**, *69*, 68–74.
8. Lau, T.; Weatherly, G.C.; Mc Lean, A. The sources of oxygen and nitrogen contamination in submerged arc welding using CaO-Al_2O_3 based fluxes. *Weld. J.* **1985**, *64*, 343–347.
9. Chai, C.S.; Eagar, T.W. Slag metal reactions in binary CaF_2-metal oxide welding fluxes. *Weld. J.* **1982**, *61*, 229–232.
10. Dallam, C.B.; Liu, S.; Olson, D.L. Flux composition dependence of microstructure and toughness of submerged arc HSLA weldments. *Weld. J.* **1985**, *64*, 140–152.
11. Coetsee, T.; Mostert, R.J.; Pistorius, P.G.H.; Pistorius, P.C. The effect of flux chemistry on element transfer in Submerged Arc Welding: Application of thermochemical modelling. *Mater. Res. Technol.* **2021**, *11*, 2021–2036. [CrossRef]

12. Mitra, U.; Eagar, T.W. Slag metal reactions during submerged arc welding of alloy steels. *Metall. Trans. B* **1984**, *15*, 217–227. [CrossRef]
13. Mitra, U.; Eagar, T.W. Slag-metal reactions during welding: Part II. Theory. *Metall. Trans. B* **1991**, *22*, 73–81. [CrossRef]
14. Zhang, J.; Coetsee, T.; Wang, C. Element transfer behaviors of fused CaF_2-SiO_2 fluxes subject to high heat input submerged arc welding. *Metall. Trans. B* **2020**, *51*, 16–21. [CrossRef]
15. Zhang, J.; Coetsee, T.; Dong, H.; Wang, C. Element transfer behaviors of fused CaF_2-SiO_2-MnO fluxes under high heat input submerged arc welding. *Metall. Trans. B* **2020**, *51*, 885–890. [CrossRef]
16. Zhang, J.; Coetsee, T.; Dong, H.; Wang, C. Element Transfer Behaviors of fused CaF_2-TiO_2 Fluxes in EH36 Shipbuilding steel during high heat input Submerged Arc Welding. *Metall. Trans. B* **2020**, *51*, 1953–1957. [CrossRef]
17. O'Brien, A. *Welding Handbook. Volume 2—Welding Processes, Part 1*, 9th ed.; American Welding Society (AWS): Miami, FL, USA, 2004; pp. 275–277.
18. Coetsee, T.; De Bruin, F.J. Improved titanium transfer in Submerged Arc Welding of carbon steel through aluminium addition. *Miner. Process. Extr. Metall. Rev.* **2021**, *43*, 1–4. [CrossRef]
19. Coetsee, T.; De Bruin, F.J. Reactions at the molten flux-weld pool interface in submerged arc welding. *High Temp. Mater. Processes.* **2021**, *40*, 421–427. [CrossRef]
20. Bailey, N. Submerged Arc Welding ferritic steels with alloyed metal powder. *Weld. J.* **1991**, *70*, 187–206.
21. Nand, S.; Singh, P.K. Effect of addition of metal powder on deposition rate, mechanical properties, and metallographic property of weld joints during Submerged Arc Welding process. *J. Mach. Form. Technol.* **2015**, *6*, 159–168.
22. Tušek, J.; Suban, M. High-productivity multiple-wire Submerged-Arc Welding and cladding with metal-powder addition. *J. Mater. Process. Technol.* **2003**, *133*, 207–213. [CrossRef]
23. Raabe, D.; Tasan, C.C.; Springer, H.; Bausch, M. From high-entropy alloys to high-entropy steels. *Steel Res. Int.* **2015**, *86*, 1127–1138. [CrossRef]
24. Moon, J.; Ha, H.-Y.; Kim, K.-W.; Park, S.-J.; Lee, T.-H.; Kim, S.-D.; Jang, J.H.; Jo, H.-H.; Hong, H.-U.; Lee, B.H.; et al. A new class of lightweight, stainless steels with ultra-high strength and large ductility. *Sci. Rep.* **2020**, *10*, 12140. [CrossRef] [PubMed]
25. Jain, H.; Shadangi, Y.; Shivam, V.; Chakravarty, D.; Mukhopadhyay, N.K.; Kumar, D. Phase evolution and mechanical properties of non-equiatomic Fe-Mn-Ni-Cr-Al-Si-C high entropy steel. *J. Alloys Compd.* **2020**, *834*, 155013. [CrossRef]
26. De, S.K.; Srikanth, S.; Saxena, A.K.; Jha, B.K. Copper bearing steels from SAIL and its application. *Int. J. Metall. Eng.* **2016**, *5*, 1–8.
27. Patel, D.; Soman, S.N. Develop a flux cored wire for submerged arc welding of Ni-Mo low alloy steel. *Sadhana* **2020**, *45*, 127. [CrossRef]
28. O'Brien, A. *Welding Handbook. Volume 4—Materials and Applications, Part 1*, 9th ed.; American Welding Society (AWS): Miami, FL, USA, 2011; pp. 256–391.
29. Coetsee, T.; De Bruin, F. Application of Copper as Stabiliser in Aluminium Assisted Transfer of Titanium in Submerged Arc Welding of Carbon Steel. *Processes* **2021**, *9*, 1763. [CrossRef]
30. Coetsee, T. Phase chemistry of Submerged Arc Welding (SAW) fluoride based slags. *Mater. Res. Technol.* **2020**, *9*, 9766–9776. [CrossRef]
31. Indacochea, J.; Blander, M.; Christensen, N.; Olson, D. Chemical reactions during Submerged Arc Welding with FeO-MnO-SiO_2 fluxes. *Metall. Trans. B* **1985**, *16*, 237–245. [CrossRef]
32. Coetsee, T.; De Bruin, F. Chemical Interaction of Cr-Al-Cu Metal Powders in Aluminum-Assisted Transfer of Chromium in Submerged Arc Welding of Carbon Steel. *Processes* **2022**, *10*, 296. [CrossRef]
33. Bale, B.R.; Chartrand, P.; Degterov, S.A.; Errikson, G. FactSage thermochemical software and databases. *Calphad* **2002**, *26*, 189–228. [CrossRef]
34. Kluken, A.O.; Grong, Ø. Mechanisms of inclusion formation in Al-Ti-Si-Mn deoxidized steel weld metals. *Metall. Trans. B* **1989**, *20*, 1335–1349. [CrossRef]
35. Bong, W.L. System and Method for Metal Powder Welding. U.S. Patent 8,946,582 B1, 18 October 2016.
36. Jung, I.; Decterov, S.A.; Pelton, A.D. Computer applications of thermodynamic databases to inclusion engineering. *ISIJ Int.* **2004**, *44*, 527–536. [CrossRef]
37. Lee, S.; Choi, J.; Jung, S.; Lee, H.; Rhee, P. Aluminium deoxidation equilibrium of liquid Fe-16 Pct Cr alloy. *Metall. Trans. B* **2005**, *36*, 414–416. [CrossRef]
38. Zhang, J.; Coetsee, T.; Basu, S.; Wang, C. Impact of gas formation on the transfer of Ti and O from TiO_2-bearing basic fluoride fluxes to submerged arc welded metals: A thermodynamic approach. *Calphad* **2020**, *71*, 102195. [CrossRef]